Aquatic Geochemistry **10:** 139–169, 2004.

The Behavior of Mixed Ca–Mn Carbonates in Water and Seawater: Controls of Manganese Concentrations in Marine Porewaters

ALFONSO MUCCI★
Department of Earth and Planetary Sciences, McGill University, 3450 University Street, Montreal, Quebec, Canada H3A 2A7

Abstract. The dissolution behavior of natural, ordered kutnahorite ($Mn_{1.14}Ca_{0.82}Mg_{0.04}Fe_{0.012}(CO_3)_2$) and a disordered, calcian rhodochrosite ($Mn_{1.16}Ca_{0.78}Mg_{0.06}(CO_3)_2$) precipitated in the laboratory was investigated in deionized distilled water and artificial seawater in both open and closed systems at 25 °C, one atmosphere total pressure, and various pCO_2s. Both solids dissolved congruently in distilled water in an open system and yielded identical long-term equilibration or extrapolated ion activity products, $IAP_{pkt} = a_{Ca^{2+}}a_{Mn^{2+}}(a_{CO_3^{2-}})^2 = 1.7(\pm 0.12)\times 10^{-21}$ or $pIAP_{pkt} = 20.77(\pm 0.03)$. This value is believed to be the thermodynamic solubility product of pseudokutnahorite. In contrast, the steady state ion concentration products, $ICP_{pkt} = [Ca^{2+}][Mn^{2+}][CO_3^{2-}]^2$, measured following the dissolution of both minerals in artificial seawater increase as the CO_2 partial pressure decreases and the $[Mn^{2+}]$:$[Ca^{2+}]$ ratio increases. These observations are interpreted as resulting from the formation of phases of different stoichiometry in response to large variations of the $[Mn^{2+}]$:$[Ca^{2+}]$ ratio in solution. These data and results of calcite-seawater equilibration experiments in the presence of various dissolved Mn(II) concentrations define the fields of stability of manganoan calcites and calcian rhodochrosites in seawater within Lippmann phase diagrams for the $CaCO_3$–$MnCO_3$–H_2O system. Results of this study reveal that the nature (i.e., mineralogy) and composition of manganese-rich carbonate phases that may form under suboxic/anoxic conditions in marine sediments are dictated by the porewater $[Mn^{2+}]$:$[Ca^{2+}]$ ratio, the abundance of calcite surfaces and reaction kinetics.

Key words: solubility, seawater, solid solutions, pseudokutnahorite, manganoan calcite, calcian rhodochrosite

1. Introduction

Kutnahorite is an isotype of dolomite and was originally described as having an ideal composition $CaMn(CO_3)_2$ and ordered cation site occupancy (Frondel and Bauer, 1955). Peacor et al. (1987), however, noted that the large ionic radius of Mn relative to Mg in dolomite leads to a distortion of the cation octahedra and a low ordering potential. An electron paramagnetic

★ Author for correspondence. E-mail: alm@eps.mcgill.ca

resonance study of natural and synthetic calcites, magnesites and dolomites containing Mn^{2+}, confirmed that it induces a distortion of the octahedral symmetry of the cationic sites in these carbonates (Wildeman, 1969, 1970). Nevertheless, Peacor et al. (1987) confirmed the existence of natural ordered kutnahorites and proposed that they are stable below 200–400 °C. The same authors also indicated that the composition of natural manganoan carbonates, including kutnahorites, are best represented by the ternary system $CaCO_3$–$MnCO_3$–$MgCO_3$ because they commonly display a continuum of compositions between calcite and rhodochrosite and contain 5–10 mol% $MgCO_3$. The presence of minor amounts of Mg may significantly influence the order–disorder relations in the kutnahorite structure (Peacor et al., 1987). The $CaCO_3$–$MnCO_3$ and $CaCO_3$–$MnCO_3$–$MgCO_3$ systems were investigated extensively at high temperatures (Capobianco and Navrotsky, 1987; de Capitani and Peters, 1981; Goldsmith and Graf, 1957, 1960).

Theoretical calculations (e.g., Lippmann, 1980; Middelburg et al., 1987), experimental studies (e.g., Bodine et al., 1965; Böttcher, 1998; Boynton, 1971; Fubini and Stone, 1983; McBeath et al., 1998; Mucci, 1988), and field observations (e.g., Jakobsen and Postma, 1989; Kulik et al., 2000; Manheim, 1982; Wartel et al., 1990) were carried out to determine phase relations in the $CaCO_3$–$MnCO_3$ system at low temperatures. Whereas thermodynamic considerations predict a large miscibility gap (Lippmann, 1980; Middelburg et al., 1987), authigenic calcian rhodochrosites of variable composition have been described (e.g., Kulik et al., 2000; Lepland and Stevens, 1998; Sternbeck and Sohlenius, 1997) and nearly continuous series of solid-solutions between the calcite and rhodochrosite end-members were precipitated experimentally (Böttcher, 1998; McBeath et al., 1998; Mucci, 1988). One possible explanation for these conflicting results is that synthetic, authigenic or diagenetic phases that precipitate at low temperatures and display a wide range of compositions are metastable. Conversely, McBeath et al. (1998) propose that within the compositional range $0.186 < x < 0.734$, the $Ca_xMn_{1-x}CO_3$ system is thermodynamically stable. Their evaluations of the excess Gibbs free energy of mixing for this system at 25 °C indicate increased stability at $x \sim 0.45$, corresponding nearly to the ideal kutnahorite composition.

Garrels et al. (1960) measured the solubility of kutnahorite following its dissolution in a CO_2-saturated distilled water solution at 25 °C. More recent measurements of the solubility and free energy of formation of natural kutnahorite in aqueous solutions at 5, 25 and 40 °C were reported by Mucci (1991). Based on the dissolution behavior of the mineral in these solutions, Mucci (1991) proposed that, over the period of the measurements, reversible equilibrium with an ordered phase was unlikely at these temperatures. Accordingly, he suggested that the solubility of the mineral was controlled by a more soluble disordered phase, a pseudokutnahorite.

The formation of authigenic, mixed Mn–Ca–Mg carbonates have been called upon to explain the composition of interstitial waters in marine and freshwater sediments (Boyle, 1983; De Lange, 1986; Emerson et al., 1980; Sayles, 1981, 1985; Suess, 1979). The presence of calcite solid solutions containing up to 50 mol% $MnCO_3$ (Calvert and Pedersen, 1996; Calvert and Price, 1970; Lynn and Bonatti, 1965; Pedersen and Price, 1982) and calcian rhodochrosites (Jakobsen and Postma, 1989; Kulik et al., 2000; Lepland and Stevens, 1998; Manheim, 1982) have been reported in marine sediments. In some cases, the authors even referred to the Mn-rich calcite phases as kutnahorite but the amount recovered was often insufficient to determine its stoichiometry and the degree of ordering. As indicated above, it is more likely that a metastable disordered phase rather than kutnahorite formed in these environments.

Despite the importance of these phases in controlling the concentration and geochemical behavior of manganese in sedimentary pore fluids, there have been very few (Böttcher, 1997a,b; McBeath et al., 1998; Mucci, 1991) attempts to determine the solubility product of mixed Ca–Mn carbonates or their domain of stability.

The dissolution behavior of a calcian rhodochrosite, approximating the stoichiometry of natural kutnahorite and thereafter referred to as pseudokutnahorite, as well as natural kutnahorite was investigated in both open and closed systems at 25 °C, one atmosphere total pressure, and various pCO_2s. Observations, results and interpretations are reported in this paper. Additional data from equilibrations of calcite in the presence of various Mn(II) concentrations and kutnahorite dissolution experiments in seawater are used to define the domains of stability of the end-member minerals in the $CaCO_3$–$MnCO_3$–seawater system.

2. Materials and Methods

2.1. SOLIDS

Samples of natural kutnahorite obtained from the Sterling Mine, New Jersey, were used in this study. Single crystal X-ray diffraction analysis of material from the same locality indicated that it is substantially ordered (Peacor et al., 1987). Physical and chemical descriptions of the solid used in this study and pre-treatments were presented previously (Mucci, 1991). Briefly, the samples were ground to a coarse powder (< 600 μm), passed through a Frantz magnetic separator, and visible contaminants were removed with tweezers under a binocular microscope (40×).

A synthetic calcian rhodochrosite (thereafter called pseudokutnahorite) was synthesized in the laboratory at room temperature. Equal volumes of CO_2-saturated 0.006 M solutions of $CaCO_3$, $MnCl_2$ and Na_2CO_3 were mixed

in a 1 l conical flask. These solutions were prepared separately by dissolution of appropriate amounts of reagent grade $CaCO_3$ (calcite), $MnCl_2{\cdot}4H_2O$, and Na_2CO_3 in distilled water while bubbling instrumental-grade (>99.99%) carbon dioxide. The $MnCl_2$ solution also contained 0.0012 M $MgCO_3$. The presence of Mg^{2+} has a strong influence on the stoichiometry of the precipitate. Peacor et al. (1987) noted that minor amounts of Mg may be necessary to generate a solvus assemblage with ordering in this dolomite-type structure at temperatures below 400 °C. The precipitation of pseudokutnahorite was initiated by bubbling a ~310 ppm CO_2/N_2 gas mixture through the mixed solution while continually stirring with a Teflon-coated magnetic bar. After approximately 3 h, a white precipitate nucleated from the solution. Degassing and stirring were maintained for at least another 3 h in order to allow crystals to age and increase in size. The crystals were then recovered by filtration of the suspension through a 0.45 μm Millipore HA filter. The filter was rinsed twice with 10 ml of distilled water and dried at room temperature. Approximately 100 mg of powder were recovered from a 750 ml total volume of the mixed solutions. Samples of both the natural kutnahorite and synthetic pseudokutnahorite were analyzed by atomic absorption spectrophotometry following their dissolution in 20 ml of concentrated HCl and dilution to 1 l in a 2000 ppm KCl solution. Aqueous standards were prepared accordingly. The composition of the natural kutnahorite corresponds to the following stoichiometry: $Mn_{1.13}Ca_{0.82}Mg_{0.040}Fe_{0.012}(CO_3)_2$ whereas that of the synthetic pseudokutnahorite prepared and used in this study is $Mn_{1.16}Ca_{0.78}Mg_{0.054}(CO_3)_2$. Preliminary X-ray diffraction refinement (i.e., Rietveld and peak width data) of the pseudokutnahorite structure revealed no significant differences between the laboratory precipitates and the natural kutnahorite. The laboratory material appears to be well crystallized as opposed to the natural material which gives broader diffraction peaks, as are commonly observed in natural dolomite (Hawthorne and Raudsepp, pers. comm.). It is worth noting that several researchers (Goldsmith, 1983; Goldsmith and Graf, 1957; Iwafuchi et al., 1983) have reported that the reflections that distinguish the ordered kutnahorite from a disordered equivalent cannot be detected with confidence by X-ray powder diffraction.

2.2. LABORATORY EXPERIMENTS

The dissolution behavior of the natural kutnahorite and synthetic pseudokutnahorite was investigated in deionized water at various CO_2 partial pressures (pCO_2s) in an open system at 25 °C. Equilibration of the natural kutnahorite in deionized water in a closed system was also carried out. Instrumental-grade carbon dioxide was used to saturate the initial solutions

for the closed-system experiments whereas commercially prepared, analyzed CO_2/N_2 gas mixtures were used to maintain the pCO_2 constant during the open-system experiments.

The dissolution of the natural kutnahorite and synthetic pseudokutnahorite in artificial seawater solutions in an open-system at various pCO_2s as well as the equilibration of kutnahorite in both supersaturated and undersaturated seawater solutions in a closed system at 25 °C were also investigated. Artificial seawater of salinity 35 was prepared according to the method of Kester et al. (1967) and the compositional data of Millero (1974). $NaHCO_3$ was withheld from the preparation when the dissolution behavior of the minerals was monitored. $NaHCO_3$ and Na_2CO_3 were added to the preparation in order to obtain a supersaturated seawater solution. The compositional evolution of seawater solutions containing various concentrations of Mn(II) (added from a stock solution of $MnCl_2$) and calcite was also monitored over time in a closed system maintained at 25 °C. Baker ''Instra-analyzed flux''® reagent grade calcite was used for these experiments. Its chemical and physical properties as well as its solubility in seawater were reported previously (Mucci, 1983).

The working principles of the open- and closed-systems were described in detail previously (Mucci, 1983, 1991). Briefly, in the open-system, 0.6–4.0 g of kutnahorite or pseudokutnahorite were suspended in 350 ml of a CO_2 or CO_2/N_2 pre-equilibrated solution maintained at 25($\pm$0.1) °C in a water-jacketed vessel. The solid was held in suspension by stirring with a motor-driven, two-bladed glass propeller mounted above the reaction vessel. Throughout the equilibration, the pCO_2 was held constant by bubbling pure CO_2 or a CO_2/N_2 gas mixture, pre-saturated with water, through the solution and aliquots of the solution were withdrawn at various intervals, filtered through a 0.45 μm HA Millipore filter and analyzed to monitor the chemical evolution of the solution and the stoichiometry of the dissolving solid.

In the closed system, 0.5 g of natural kutnahorite or calcite was added to 60 ml of filtered CO_2-saturated deionized water or 320 ppm CO_2/N_2-equilibrated seawater solutions in opaque polycarbonate bottles. In the latter case, the initial solutions were undersaturated or supersaturated with respect to the solid in order to verify the reversibility of the reaction. The bottles were placed on a rotating table immersed in a constant temperature water bath at 25 °C. After various periods of equilibration, the bottles were stabilized and the solid allowed to settle before the pH of the solution was measured. A combination electrode was inserted in the neck of the bottle as soon as it was opened. The electrode was fitted with a piece of Tygon® tubing and Parafilm® to form an air-tight seal and prevent CO_2 exchange with the atmosphere. Immediately after the pH measurement, the solution was drawn from the bottle using a 60 cm^3 syringe, filtered through a 0.45 μm HA Millipore filter, and analyzed as described below.

2.3. ANALYSES

The concentrations of dissolved Ca, Mn and Mg in each sample were determined by atomic absorption spectrophotometry (Perkin-Elmer® model 5100) in an air-acetylene flame following appropriate dilution with a 10% HCl solution. The precision of these analyses is estimated to be better than $\pm 3\%$. In the case of seawater solutions, Ca concentrations were determined by potentiometric titration with EGTA (Lebel and Poisson, 1976) with a precision of $\pm 0.4\%$. Titration alkalinity, A_t, was determined by potentiometric titrations using standardized dilute HCl solutions with a precision of better than 0.4%. In the deionized water solutions, the titration alkalinity is equal to the carbonate alkalinity (i.e., $A_c = [HCO_{3^-}] + 2[CO_3^{2-}]$). For the seawater solutions, the carbonate alkalinity was calculated from titration alkalinity after subtracting the contribution of boric acid (Dickson, 1981). The pH measurements were carried out, prior to sampling, with a combination glass electrode (Radiometer® GK2401C) calibrated before and after each measurement with a set of three NIST-traceable buffers (4.008, 6.865 and 7.413 at 25 °C, Bates 1973) as well as a TRIS buffer solution (8.074 at 25 °C and $S = 35$, Hansson, 1973, Millero et al., 1993) for artificial seawater measurements. pH measurements on both the NIST and TRIS buffer scales in combination with carbonate alkalinities, when used with the appropriate constants (Dickson and Millero, 1987; Goyet and Poisson, 1989; Hansson, 1973; Mehrbach et al., 1973; Millero, 1979; Roy et al., 1993), give independent estimates of the concentrations of carbonic acid species in seawater. Carbonate ion concentrations estimated using both sets of measurements and constants generally agreed to within $\pm 5\%$. The reproducibility of the pH measurements was estimated to be better than ± 0.005 pH units.

2.4. SPECIATION CALCULATIONS

The free concentration of ionic species involved in the reactions carried out in distilled water was calculated using a slightly modified version of WATEQF (Ball et al., 1980; Plummer et al., 1976). Free-ion activity coefficients derived from WATEQF are estimated from an extended Debye-Hückel equation (Plummer and Busenberg, 1982). Association constants for the various species considered in the calculations are presented in Table I.

3. Results

3.1. DEIONIZED WATER

Experimental results of the open-system measurements in distilled water are presented in Table II. In two of the three cases where kutnahorite was used as the starting material, the solid first underwent a congruent dissolution period.

Table I. Summary of relevant thermodynamic data at 25 °C

Reaction	−log K	Reference
$CaHCO_3^+ \Longleftrightarrow Ca^{2+} + HCO_3^-$	1.11	Plummer and Busenberg (1982)
$MgHCO_3^+ \Longleftrightarrow Mg^{2+} + HCO_3^-$	1.07	Ball et al. (1980)
$MnHCO_3^+ \Longleftrightarrow Mn^{2+} + HCO_3^-$	1.28	Lesht and Bauman (1978)
$NaHCO_3^o \Longleftrightarrow Na^{2+} + HCO_3^-$	−0.25	Garrels et al. (1961)
$CaCO_3^o \Longleftrightarrow Ca^{2+} + CO_3^{2-}$	3.22	Plummer and Busenberg (1982)
$MgCO_3^o \Longleftrightarrow Mg^{2+} + CO_3^{2-}$	2.98	Ball et al. (1980)
$NaCO_3^+ \Longleftrightarrow Na^+ + CO_3^{2-}$	1.27	Garrels and Thompson (1962)
$MnCl^- \Longleftrightarrow Mn^{2+} + Cl^-$	0.61	Ball et al. (1980); Gammons and Seward (1996)
$CO_2(g) \Longleftrightarrow CO_2(aq)$	1.468	Plummer and Busenberg (1982)
$CO_2(aq) + H_2O \Longleftrightarrow H^+ + HCO_3^-$	6.352	Plummer and Busenberg (1982)
$HCO_3^- \Longleftrightarrow H^+ + CO_3^{2-}$	10.329	Plummer and Busenberg (1982)

Extrapolation of the congruent dissolution data (i.e., pH, A_c, $[Ca^{2+}]$, $[Mn^{2+}]$; Exp. #24, 25; see Figure 1a and c) obtained over a 2–3 day period to infinite time yields ion activity products that are identical to the thermodynamic solubility product reported by Mucci (1991) for the kutnahorite mineral. The application of inverse time plots to extrapolate the congruent dissolution behavior of solid phases to infinite time and equilibrium conditions is not suitable to all systems and requires that the kinetics of the dissolution process be established. It may yield a unidirectional "kinetic" steady state solution composition that does not reflect a true, reversible equilibrium. Nevertheless, this approach has been applied successfully to many carbonate minerals (e.g., Garrels et al., 1960), including calcite (e.g., Plummer and Mackenzie, 1974) and kutnahorite (e.g., Mucci, 1991 and this study) for which results of conventional, long-term equilibrations and short-term dissolution extrapolations have been shown to be coincident.

After about 4 days ($t^{-0.5} \sim 0.013$), the stoichiometry of these solutions remained the same or deviated slightly from that of the dissolving solid (i.e., $[Mn^{2+}]/([Ca^{2+}] + [Mn^{2+}])$ remained the same at 0.55 in most experiments but decreased slightly to 0.48 in Exp. #29) while the pH, alkalinity, $[Mn^{2+}]$ and $[Ca^{2+}]$ increased rapidly (Figure 1a). A steady state solution composition was not reached over the duration of these experiments (i.e., 8–16 days). These dissolution data were extrapolated to infinite time using inverse time plots ($t^{-0.5} = 0$, Figure 1a and b) in order to obtain the steady state solution compositions. In contrast to kutnahorite, the synthetic pseudokutnahorite dissolved congruently and a steady state IAP was reached within a few days (see Table II). The pseudokutnahorite dissolution data obtained prior to the steady state being reached extrapolate well to the long-term equilibration values when plotted against $t^{-0.5}$ and, thus, bolsters the validity of this

Table II. Measurements of open-system solubility of pseudokutnahorite in deionized water at 25 °C

Exp.#	Solid	W_{solid} (g)	pCO_2 (atm)	time (h)	$[Ca^{2+}]$ (mol $l^{-1} \times 10^{-5}$)	$[Mg^{2+}]$	$[Mn^{2+}]$	A_c (meq l^{-1})	pH (NBS)	IAP_{pkt} (10^{-21})	IAP_{rh} (10^{-11})
24	Kut[a]	2.612	1	∞/391[b]	96	119	6.3	4.14	5.53	1.88/1.92	4.78
25	Kut	3.988	1	∞/195	77	107	5.2	3.76	5.58	1.50/1.83	4.86
29	Kut	1.280	1	744	101	94	4.7	4.65	5.486	1.64/1.64	3.85
54	SPK[a]	1.497	0.30	48	67	77	–	3.29	5.744	1.65/1.66	4.29
				72	71	77	–	3.23	5.728	1.58/1.58	4.11
				144	78	77	–	3.21	5.716	1.61/1.61	3.94
56	SPK	1.500	0.02	168	34	34	–	1.120	6.496	1.90/1.90	4.37
				217	35	33	–	1.096	6.488	1.73/1.74	4.00
57	SPK	1.499	0.30	168	55	84	–	2.90	5.813	1.61/1.75	4.91
				192	55	84	–	2.89	5.806	1.60/1.82	4.88
				216	55	83	–	2.88	5.805	1.50/1.63	4.73
				312	56	88	–	2.89	5.791	1.54/1.69	4.85
58	SPK	1.504	1	72	99	137	–	4.40	5.442	1.63/1.75	4.74
				144	99	138	–	4.40	5.440	1.63/1.68	4.69
				168	99	138	–	4.38	5.442	1.61/1.69	4.77
				192	103	143	–	4.27	5.448	1.71/1.80	4.91
				217	102	141	–	4.28	5.443	1.60/1.68	4.65
				241	100	138	–	4.27	5.436	1.54/1.62	4.65

[a]Kut: Natural kutnahorite, SPK: synthetic pseudokutnahorite.

[b]∞/ Time means that equilibrium solution parameters were extrapolated to infinite time using inverse time plots from data acquired over variable periods of time.

[c]IAP_{pkt}: Ion activity product for pseudokutnahorite = $a\mathrm{Mn}^{2+}\ a\mathrm{Ca}^{2+}\ (a\mathrm{CO}_3^{2-})^2$ according to equation (2), and for the mixed carbonate according to the stoichiometry of the dissolving solid, $[(a\mathrm{Ca}^{2+})^x\ (a\mathrm{Mn}^{2+})^{(1-x)}\ (a\mathrm{CO}_3^{2-})]^2$ according to equation (6).

[d] IAP_{rh}: Ion activity product for rhodochrosite = $a\mathrm{Mn}^{2+}\ a\mathrm{CO}_3^{2-}$.

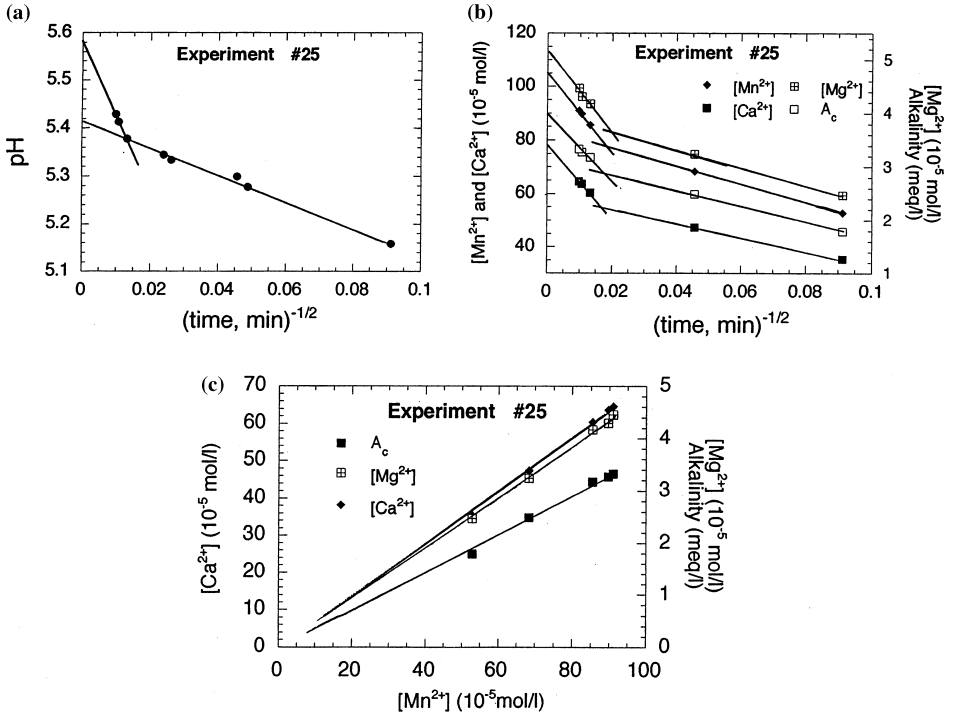

Figure 1. Inverse time plots and extrapolations of (a) pH, (b) $[Ca^{2+}]$, $[Mn^{2+}]$, $[Mg^{2+}]$, and carbonate alkalinity (A_c) and (c) stoichiometry of the solution following the dissolution of kutnahorite in CO_2-saturated deionized, distilled water at 25 °C in an open-system (Exp. #25).

approach for this mineral system. The reaction path of both dissolution reactions in distilled water moves up almost vertically from the abscissa of a Lippmann diagram (Lippmann, 1980) at a Mn mole fraction corresponding almost exactly to the stoichiometry of the dissolving solid (not shown). This is the behavior expected of a solid solution undergoing congruent dissolution (Glynn et al., 1990; Kornicker et al., 1991).

Results of the closed-system equilibration measurements are presented in Table III. Included in the table are results presented earlier by Mucci (1991) for the first 69 days of equilibration and from which the solubility product of pseudokutnahorite was crudely estimated. The data indicate that beyond an equilibration period of 1 month, the dissolved manganese concentration decreases rapidly with time. This observation is associated with an increase in pH and decrease in alkalinity of the solution. Visual examination of the recovered solids showed them to be covered by a brown coating that could have been rhodochrosite ($MnCO_3$) or a manganese oxide. The formation of rhodochrosite can clearly be dismissed as the solubility controlling phase because, after longer periods of equilibration (up to 632 days, results not

Table III. Closed-system equilibration of natural kutnahorite in deionized water at 25 °C

Time (day)	$[Ca^{2+}]$ (mol $l^{-1} \times 10^{-5}$)	$[Mn^{2+}]$	$[Mg^{2+}]$	A_c (meq l^{-1})	pH (NBS)	IAP_{pkt}[a] (10^{-21})	IAP_{rh} (10^{-11})	IAP_{cc}[a] (10^{-10})	$\Sigma\Pi^{\circ}$[b] (10^{-9})
6	67	80	3.63	3.19	5.458	0.44	2.26	0.20	0.042
8	73	80	5.82	3.17	5.527	0.58	2.40	0.24	0.048
13	67	81	3.68	3.21	5.649	1.07	3.55	0.30	0.066
18	93	85	3.48	3.25	5.805	2.76	5.22	0.53	0.105
20	71	81	3.68	3.26	5.836	2.75	5.59	0.49	0.105
23	71	82	3.80	3.38	5.758	2.09	4.83	0.43	0.092
33	69	79	3.55	3.17	6.154	9.65	10.9	0.89	0.20
69	65	49	–	2.52	6.825	93	26.2	3.55	0.62
93	60	36	–	2.34	7.022	142	28.8	4.93	0.78
136	72	8.2	3.48	1.604	7.360	96	10.4	9.23	1.03
183	70.3	1.35	3.76	1.511	7.916	179	5.85	30.6	3.12

[a]IAP_{cc}: Ion activity product of a Ca^{2+} aCO_3^{2-}.
[b]$\Sigma\Pi^{\circ} = \{aMn^{2+} + aCa^{2+}\}^{*}aCO_3^{2-}$.

shown), the manganese concentration decreased to below our detection limit (i.e., < 0.1 ppm). It is therefore more likely that Mn(II) was oxidized and precipitated as an oxide. The oxidation of Mn(II) is known to be catalyzed by solid surfaces, including carbonates (Boynton, 1971), in the presence of oxygen. Similarly, the oxidation of Fe(II) in solution is catalyzed in the presence of calcite surfaces (Clarke et al., 1985; Loeppert and Hossner, 1984; Mettler, 2002). Despite the fact that solutions were pre-equilibrated with pure CO_2 or a CO_2/N_2 mixture, the presence of oxygen was not likely excluded from the initial solution. Alternatively, oxygen may have diffused through the walls of the bottles during the equilibration period. Although results of the closed-equilibration experiments yield similar IAP_{pkt} values after 13–23 days of equilibration (see Table III), before the onset of the $[Mn^{2+}]$ decrease, they cannot be clearly interpreted. Furthermore, a mass balance of the carbon in the system cannot be established, as both the total dissolved inorganic carbon concentration (ΣCO_2) and pCO_2 decrease progressively throughout the equilibration period.

The thermodynamic solubility product of pseudokutnahorite was calculated from the long-term steady state or extrapolated ion activity product (IAP, Table II) of the solutions which corresponds to the equilibrium constant for the dissolution reaction of the mineral into its ionic components:

$$CaMn(CO_3)_{2(pkt)} \Longleftrightarrow Ca^{2+} + Mn^{2+} + 2CO_3^{2-} \quad (1)$$

Thus,

$$\mathrm{IAP_{pkt}} = a\mathrm{Ca}^{2+}\ a\mathrm{Mn}^{2+}\ (a\mathrm{CO_3^{2-}})^2, \tag{2}$$

$$= \{[\mathrm{Ca}^{2+}]_\mathrm{f}[\mathrm{Mn}^{2+}]_\mathrm{f}[\mathrm{CO_3^{2-}}]_\mathrm{f}^2\}\{\gamma_\mathrm{f}(\mathrm{Ca}^{2+})\gamma_\mathrm{f}(\mathrm{Mn}^{2+})\gamma_\mathrm{f}(\mathrm{CO_3^{2-}})^2\}, \tag{3}$$

and, at equilibrium:

$$\mathrm{IAP_{pkt}} = K^\mathrm{o}_\mathrm{pkt}, \qquad \mathrm{p}K^\mathrm{o}_\mathrm{pkt} = -\log K^\mathrm{o}_\mathrm{pkt}, \tag{4}$$

where $K^\mathrm{o}{}_\mathrm{pkt}$ is the equilibrium thermodynamic solubility product of pseudokutnahorite and a_i, $[\mathrm{i}]_\mathrm{f}$, and $\gamma_\mathrm{f}(\mathrm{i})$ are, respectively, the activity, free (i.e., uncomplexed) concentration, and free activity coefficient of species i. Conventionally, the activity of the one-phase solid is equal to unity.

If, on the other hand, the K^o is calculated according to the stoichiometry of the dissolving solid (i.e., Ca:Mn $\neq$ 1, but equal to the steady state solution composition), such that:

$$\mathrm{Ca}_{2x}\mathrm{Mn}_{2(1-x)}(\mathrm{CO_3})_2 \Longleftrightarrow 2x\mathrm{Ca}^{2+} + 2(1-x)\mathrm{Mn}^{2+} + 2\mathrm{CO_3^{2-}}, \tag{5}$$

then,

$$K^\mathrm{o} = [(a\mathrm{Ca}^{2+})^x(a\mathrm{Mn}^{2+})^{1-x}(a\mathrm{CO_3^{2-}})]^2, \tag{6}$$

and the values of the solubility constant only increase marginally (i.e., $< 5\%$, Table II) and are well within the cumulative uncertainty of the measurements which are estimated at $\pm 11\%$.

3.2. SEAWATER

Results of the open-system measurements in seawater are presented in Table IV. Like its behavior in distilled water, a constant ion concentration product (ICP) was reached in solutions reacted with the synthetic pseudokutnahorite whereas steady state solution parameters had to be extrapolated to $t^{-0.5} = 0$ when natural kutnahorite was used as the starting material (e.g., Exp. #45; Figure 2)

$$\mathrm{ICP_{pkt}} = [\mathrm{Ca}^{2+}][\mathrm{Mn}^{2+}][\mathrm{CO_3^{2-}}]^2. \tag{7}$$

The steady-state $\mathrm{ICP_{pkt}}$ values increase as the $\mathrm{pCO_2}$ of the experimental solution decreases and the $[\mathrm{Mn}^{2+}]$:$[\mathrm{Ca}^{2+}]$ ratio increases (Table IV). The steady-state $[\mathrm{Mn}^{2+}]$ increases with $\mathrm{pCO_2}$ because more of the mineral dissolves before saturation is reached.

All closed-system solubility measurements in seawater were carried out with the natural kutnahorite from both undersaturated and supersaturated solutions equilibrated at a $\mathrm{pCO_2} = 0.03\%$. Unlike the distilled water, closed-

Table IV. Measurements of open-system solubility of pseudokutnahorite in seawater at 25 °C

Exp.#	Solid	W_{solid} (g)	pCO_2 (%)	time (h)	$[Ca^{2+}]$ (mmol kg^{-1})	$[Mn^{2+}]$ (μmol kg^{-1})	A_t (meq kg^{-1})	pH (sws)	ICP_{pkt} (10^{-17})	ICP_{rh} (10^{-9})	$\Sigma\Pi$ (10^{-8})
28	Kut[a]	1.499	100	∞/73[b]	12.5	1650	6.36	5.24	3.18[c]	2.05[d]	1.76[e]
33	Kut	1.505	100	∞/145	13.3	1650	7.02	5.22	3.75	2.16	1.96
42	Kut	2.005	100	∞/265	12.4	1650	6.50	5.23	3.20	2.06	1.75
66	SPK[a]	1.400	100	168–264	15.6	1730	8.05	5.42	14.7	4.04	4.05
47	Kut	2.000	30	∞/264	12.0	1220	4.77	5.60	6.60	2.59	2.81
51	Kut	1.999	30	∞/265	12.2	1290	4.99	5.57	6.88	2.70	2.82
62	SPK	0.600	30	168–362	12.4	1830	5.28	5.71	20.5	5.52	4.28
43	Kut	2.001	3.0	∞/265	11.1	569	2.13	6.55	44.6	4.78	9.80
46	Kut	2.003	3.0	∞/264	11.9	747	2.22	6.38	31.9	4.47	7.57
48	Kut	2.000	3.0	∞/216	11.7	571	2.23	6.54	50.1	4.94	10.6
52	Kut	2.202	3.0	∞/265	11.2	617	2.31	6.48	41.4	4.78	9.15
64	SPK	1.404	3.0	5–264	11.5	822	2.57	6.29	30.4	4.66	7.00
32	Kut	1.500	0.30	∞/314	10.8	306	1.185	7.06	74.8	4.60	16.7
34	Kut	1.500	0.30	∞/432	11.0	261	0.965	7.11	52.8	3.57	15.4
41	Kut	2.001	0.30	∞/243	10.8	292	1.077	7.07	60.3	4.04	15.4
45	Kut	2.001	0.30	∞/242	11.0	275	1.055	7.10	61.5	3.92	16.1
44	Kut	2.000	0.03	∞/240	10.8	138	0.525	7.58	54.3	2.63	20.9
49	Kut	2.001	0.03	∞/264	10.5	128	0.498	7.58	43.7	2.31	19.2
65	SPK	1.400	0.03	24-264	10.64	157	0.722	7.60	133	4.43	30.5

[a]Kut: Natural kutnahorite, SPK: synthetic pseudokutnahorite.

[b]∞/Time means that equilibrium solution parameters were extrapolated to infinite time using inverse time plots from data acquired over variable periods of time.

[c]ICP_{pkt}: Ion concentration product for pseudokutnahorite = $[Mn^{2+}][Ca^{2+}][CO_3^{2-}]^2$ in $mol^4\ kg^{-4}$ sw.

[d]ICP_{rh}: Ion concentration product for rhodochrosite = $[Mn^{2+}][CO_3^{2-}]$ in $mol^2\ kg^{-2}$ sw.

[e]$\sum\prod = ([Mn^{2+}] + [Ca^{2+}])*[CO_3^{2-}]$ in $mol^2\ kg^{-2}$ sw.

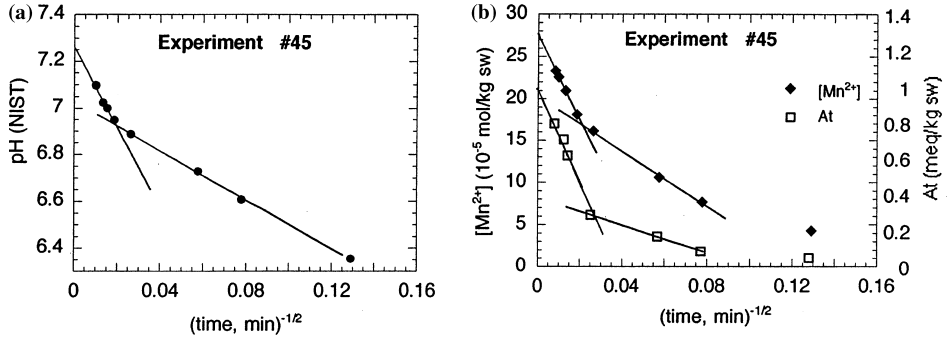

Figure 2. Inverse time plots and extrapolations of (a) pH, (b) $[Mn^{2+}]$ and titration alkalinity (A_t) following the dissolution of kutnahorite in seawater at 25 °C in an open-system and a pCO_2 of 0.30% (Exp. #45).

Table V. Closed-system equilibration of natural kutnahorite in seawater ($S = 35.0$) at 25 °C

U/S–Time* (day)	$[Ca^{2+}]$ (mmol kg^{-1})	$[Mn^{2+}]$ (μmol kg^{-1})	A_t (meq kg^{-1})	A_c (meq kg^{-1})	pH (sws)	ICP_{pk} (10^{-16})	$pICP_{pk}$
U-0	10.19	17	0.819	0.770	7.620	2.00	15.70
S-0	10.18	85	0.820	0.771	7.620	10.1	15.00
U-122	10.67	33	0.893	0.861	7.415	2.14	15.67
U-199	10.07	36	0.859	0.820	7.510	2.88	15.54
S-199	10.22	89	0.858	0.819	7.510	7.34	15.13
U-330	10.35	41	0.893	0.854	7.510	3.81	15.42
S-330	10.27	88	0.892	0.855	7.480	7.09	15.15
U-931	10.20	43	0.914	0.873	7.535	4.51	15.35
S-931	10.19	71	0.892	0.852	7.515	6.60	15.18

*Time of equilibration from undersaturated or supersaturated solutions.

system experiments (Table III), a mass balance of carbon was maintained throughout the equilibration period in seawater. Calculated ICP values of the individual batch solutions withdrawn throughout the experiment had not yet converged after 931 days of equilibration (Table V). Extrapolation of the available data from undersaturation and supersaturation to $t^{-0.5} = 0$ (Figure 3) converge at ICP^*_{pkt} of 6.0×10^{-16} mol^4 kg^{-4} sw or $pICP^*_{pkt} = 15.22$, in very good agreement with the values obtained in the open-system at low pCO_2 (i.e., $pCO_2 < 3.0\%$; $6 \pm 3 \times 10^{-16}$ mol^4 kg^{-4} sw) and low $[Mn^{2+}]$:$[Ca^{2+}]$ ratios. This steady state ICP^*_{pkt} does not correspond to the stoichiometric solubility constant of pseudokutnahorite that can be derived from the thermodynamic constant obtained in pure water (i.e., $K^o_{pkt} = 1.7 \times 10^{-21}$; this study) and estimates of the total activity coefficients of the constituent ions in seawater:

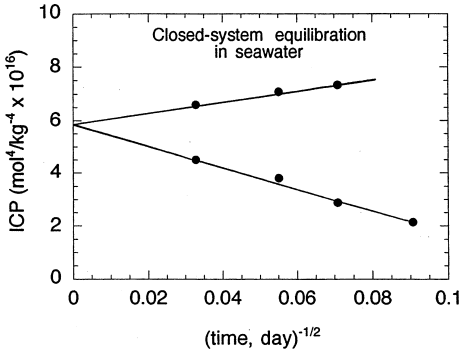

Figure 3. Ion concentration product, $[Mn^{2+}][Ca^{2+}][CO_3^{2-}]^2$, of the seawater solution during the closed-system equilibration with kutnahorite at 25 °C as a function of $t^{-0.5}$.

$$K^*_{pkt} = \frac{K^o_{pkt} * \theta^4}{\gamma t(Ca^{2+})\gamma t(Mn^{2+})\gamma t(CO_3^{2-})^2}, \tag{8}$$

where θ is a conversion factor (mol^{-1} kg sw to mol^{-1} kg H_2O; equal to $1-S/1000$ or 0.965) and γ_t(i) is the total ion activity coefficient of the ion. Values of $\{\gamma_t(Ca^{2+})\gamma_t(Mn^{2+})\gamma_t(CO_3^{2-})^2\}$ estimated from various models vary from 2.82×10^{-5} (Franklin and Morse, 1983; Millero and Schreiber, 1982; ion–pairing model) to 6.51×10^{-5} (Millero and Pierrot, 1998; specific interaction or Pitzer model) and yield K^*_{pkt} values between 5.2 and 2.3×10^{-17} mol^4 kg^{-4} sw, one order of magnitude less than the value obtained in the closed–system and at low pCO_2 (i.e., pCO_2 < 3.0%) in the open-system but similar to the value obtained with kutnahorite in the open-system at high pCO_2 (i.e., pCO_2 > 3.0%; $5 \pm 2 \times 10^{-17}$ mol^4 kg^{-4} sw; see Table IV).

4. Discussion

4.1. MINERAL SATURATION, A TRULY DYNAMIC EQUILIBRIUM

A most fascinating aspect of this study was the dissolution and equilibration behavior of the kutnahorite in the open and closed systems, specifically the formation and saturation of the solution with respect to the disordered phase (i.e., pseudokutnahorite) from a highly undersaturated solution. This is a vivid example of the differential behavior of irreversible and reversible reactions and the dynamic nature of the equilibrium state (a metastable state in this particular case). In both deionized water and seawater, open-system experiments in which the ordered kutnahorite was the starting material, the composition of the solutions displayed an abrupt change in dissolution kinetics and evolved beyond the solubility of this mineral (Figures 1 and 2). In the initial and slower stage of the dissolution in distilled water, the mineral dissolved congruently and, in some cases (e.g., Exp. #24, 25, Table II;

Figure 1), these initial data could be extrapolated to the solubility product of kutnahorite (Mucci, 1991). After approximately 4 days (i.e., $t^{-0.5} = 0.02$), the Ca^{2+} and Mg^{2+} concentrations, the carbonate alkalinity, and pH increased suddenly and more rapidly than during the first stage of the dissolution (see Figure 1a and b and 2a and b) until they reached (or were extrapolated to) a reproducible and much higher IAP_{pkt} or ICP_{pkt}. A possible explanation is that once saturation with respect to the ordered kutnahorite is achieved, the system is poised temporarily because, as indicated earlier, the ordered mineral cannot precipitate from the solution at 25 °C (the transient-state is dictated by an irreversible reaction) and a reversible reaction that involves a disordered mineral (e.g., pseudokutnahorite) proceeds to equilibrium such as

$$MnCa(CO_3)_{2(kt)} \rightarrow Mn^{2+} + Ca^{2+} + 2CO_3^{2-} \leftrightarrow MnCa(CO_3)_{2(pkt)}. \quad (9)$$

A dissolution experiment carried out under similar conditions with dolomite ($CaMg(CO_3)_2$; results not shown) also resulted in a two-step dissolution, a steady state IAP was maintained for a few hours before the Ca^{2+} and Mg^{2+} concentrations, the carbonate alkalinity, and pH suddenly increased sharply well beyond the dolomite solubility constant.

4.1.1. Solubility of Pseudokutnahorite in Dilute Solutions

Assuming that the interpretation of the reaction path described above is accurate and a solid solution, approximating pseudokutnahorite in composition, determines the saturation state of the solutions, the average thermodynamic solubility constant obtained from the seven independent measurements presented in Table II is $1.70\ (\pm 0.12) \times 10^{-21}$ or a pK^{o}_{pkt} of 20.77 ± 0.03. It is interesting to note that, despite the experimental artefacts, the ICP_{pkt} values measured in the closed-system (see Table III) for equilibration periods of 13–23 days, prior to manganese depletion in solution, were similar (i.e.,$-\log ICP_{pkt} = 20.70 \pm 0.17$).

Accordingly, the Gibbs free energy of the reaction (equation (1)) can be calculated from the following relation:

$$\Delta G^{o}_{rx} = -RT \ln K^{o}_{pkt}, \quad (10)$$

where R is the gas constant ($= 8.413$ J K^{-1} mol^{-1}) and T is in Kelvin. The value calculated from the solubility constant at 25 °C is 118.55 (± 0.18) kJ mol^{-1}. This value and the free energy of formation of the species involved in the reaction (equation (1)) can then be used to calculate the standard free energy of formation of pseudokutnahorite:

$$\Delta G^{o}_{f-pkt} = \Delta G^{o}_{f}(Ca^{2+}) + \Delta G^{o}_{f}(Mn^{2+}) + 2\Delta G^{o}_{f}(CO_3^{2-}) - \Delta G^{o}_{rx}. \quad (11)$$

Substituting the value of $\Delta G^{o}{}_{rx}$ (equation 10) and the ΔG^{o}_{f} of the ions (Robie et al., 1978) into equation (11), $\Delta G^{o}_{f-pkt} = -1955.9(\pm 0.2)$ kJ mol^{-1} at 25 °C and one atmosphere total pressure.

4.1.2. *Compositional Dependence of the Steady State ICP$_{pkt}$* in Seawater

As indicated above and in Table IV, the steady state ICP_{pkt} values obtained in the open-system seawater experiments decrease with increasing pCO_2. The behavior most likely reflects the formation and equilibration with a phase of different stoichiometry or mineralogy which is dictated by the $[Mn^{2+}]$:$[Ca^{2+}]$ ratio of the solutions or stoichiometric saturation (Thorstenson and Plummer, 1997). Unfortunately, the nature (i.e., composition and mineralogy) of the solubility-controlling phase could not readily be determined with instrumentation at our disposal because, under the experimental conditions, it is much too thin. In the absence of this information, the solution data are most easily interpreted using Lippmann phase diagrams (Glynn and Reardon, 1990; Kulik et al., 2000; Lippmann, 1980) for the $CaCO_3$–$MnCO_3$–H_2O system. According to this convention, the aqueous solution composition at equilibrium is defined by

$$\Sigma\Pi_{eq} = ([Ca^{2+}] + [Mn^{2+}])([CO_3^{2-}]), \tag{12}$$

where $\Sigma\Pi$ is the total stoichiometric solubility product. In the two mineral phase component system (i.e., calcite–rhodochrosite) under consideration, the composition of the solution in equilibrium with the solid solution which forms from this solution, the *solutus*, is given by (Gamsjäger et al., 2000; Lippmann, 1980):

$$\Sigma\Pi_{rh} = \frac{K^{*}_{rh} X_{S(Mn)} \exp\{a(1 - X_{S(Mn)})^2\}}{X_L(Mn)}, \tag{13}$$

$$\Sigma\Pi_{cc} = \frac{K^{*}_{cc}(1 - X_{S(Mn)} \exp\{a X_{S(Mn)})^2\}}{X_L(Ca)}, \tag{14}$$

where $K^{*}{}_{cc}$ and $K^{*}{}_{rh}$ are, respectively, the stoichiometric solubility constants of calcite (4.4×10^{-7} mol^2 kg^{-2} sw, Mucci, 1983) and rhodochrosite (3.2×10^{-9} mol^2 kg^{-2} sw, Johnson, 1982) in seawater at 25 °C and $S = 35$, $X_{S(Mn)}$ and $X_{L(Mn)}$ are, respectively, the mole fraction of Mn (= Mn/(Ca + Mn)) in the solid solution and aqueous solution, and a is the Guggenheim/Margules parameter. The Guggenheim/Margules parameter was estimated by Lippmann (1980, $a = 3.2248$) from the excess enthalpy of mixing of the end-member minerals for the case of a regular solution.

The *solidus* was calculated assuming a regular solid solution behavior according to:

$$\Sigma\Pi = K^*_{cc}(1 - X_{S(\mathrm{Mn})}) \exp\{aX_{S(\mathrm{Mn})}{}^2\} + K^*_{rh}X_{S(\mathrm{Mn})} \exp\{a(1 - X_{S(\mathrm{Mn})}{}^2\}. \tag{15}$$

The theoretical Guggenheim/Margules parameter is greater than 2 and implies the presence of a stable miscibility gap. The mole fraction, X^{gap}, at maximum stable solid solution is related to this parameter by (Lippmann, 1980, 1982):

$$\ln(1 - X^{gap}) - \ln X^{gap} = a(1 - 2X^{gap}). \tag{16}$$

An iterative solution to equation (16) reveals that the miscibility gap extends nearly across the entire range of compositions, from $X_{S(\mathrm{Mn})} = 0.053$ to 0.947. The horizontal line that joins these two points and crosses the *solidus* defines the peritectic line at log $\Sigma\Pi = -6.373$. Given the amount of calcium that can be accommodated in a stable calcian rhodochrosite, equation (13) can be simplified to:

$$\Sigma\Pi_{rh} = \frac{K^*_{rh}}{X_{L(\mathrm{Mn})}}. \tag{17}$$

Finally, the eutectic is given by

$$X_{L(\mathrm{Mn})} = \frac{K^*_{rh}}{(K^*_{rh} + K^*_{cc})} = 0.0072. \tag{18}$$

The Lippmann phase diagram for the system $CaCO_3$–$MnCO_3$–H_2O is presented in Figure 4a and b. The *soluti* and *solidus* curves are plotted, respectively, as a function of the mole fraction of manganese in the aqueous solution and the solid. Horizontal tie lines between the *solutus* and *solidus* join the solid mole fractions and aqueous mole fractions at equilibrium. Note, however, that other studies (Böttcher, 1997b, 1998; Jakobsen and Postma, 1989; McBeath et al., 1988) revealed that the theoretical Guggenheim/Margules parameter derived by Lippmann (1980) may be too high and the application of a regular solid solution model may be too simple (e.g., Capobianco and Navrotsky, 1987).

The reaction describing the dissolution of the kutnahorite and synthetic pseudokutnahorite in seawater is represented by equation (5) for which the mass expression is

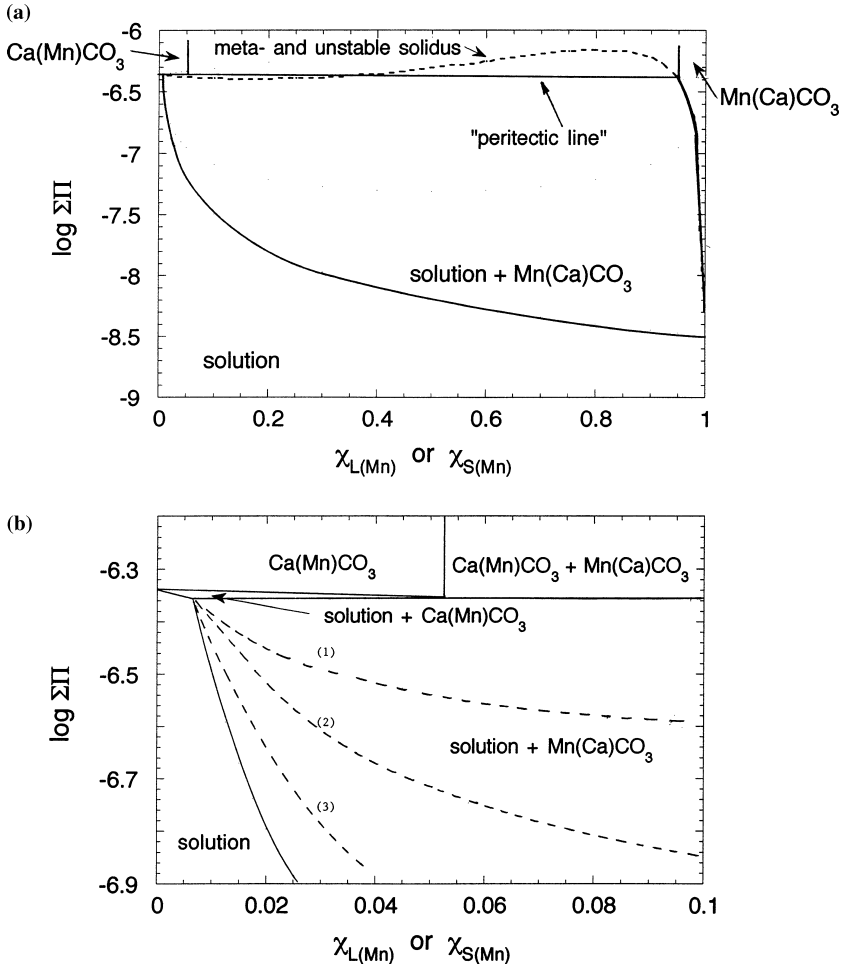

Figure 4. Solubility relations in the system $CaCO_3$–$MnCO_3$–H_2O at 25 °C in seawater. (a) The *soluti* of calcite (cc) and rhodochrosite (rh) are obtained from equations (13), (14) and (17). The calcian rhodochrosite *solidus* was calculated assuming a regular solid solution with a Guggenheim/Margules parameter $\alpha = 3.23$ (equation (15)). Horizontal tie lines between the *solutus* and *solidus* join the solid mole fractions and aqueous mole fractions at equilibrium. (b) Expanded version of the Lippmann phase diagram for $X_{S(Mn)} < 0.1$. Dashed lines represent stoichiometic saturation with respect to the following regular solid solutions: (1) $Ca_{0.25}Mn_{0.75}CO_3$; (2) $Ca_{0.5}Mn_{0.5}CO_3$; (3) $Ca_{0.75}Mn_{0.25}CO_3$.

$$K_{ss}^{*} = [Ca^{2+}]^{x}[Mn^{2+}]^{(1-x)}[CO_3^{2-}]. \tag{19}$$

The relationship between the stoichiometric saturation constant and the solubility products of the pure end-member constituents is given by

$$K_{ss}^{*} = (K_{cc}^{*})^{x}(K_{rh}^{*})^{(1-x)}X^{x}(1-X)^{(1-x)}\exp(aX(1-X)). \tag{20}$$

The stoichiometric saturation can then be represented on a Lippmann diagram (Glynn and Reardon, 1990; Glynn et al., 1990; Kornicker et al., 1991) by:

$$\Sigma\Pi_{ss} = \frac{K^*_{ss}}{\{(X_{L(Ca)})^x (X_{S(Mn)})^{(1-x)}\}}. \quad (21)$$

$\Sigma\Pi_{ss}$ for a given solid solution composition yields a curve on the Lippmann diagram, whereas $\Sigma\Pi_{eq}$ represents a single point. The $\Sigma\Pi_{ss}$ curves for solid solutions of various compositions are represented by the dashed lines in Figures 4b and 6. Representative reaction paths of the dissolution reactions of the two solids at various pCO_2 in seawater are shown in Figure 5.

All of the data presented in Tables III and IV plot for $0.01 < X_{L(Mn)} < 0.13$ and are reproduced on a logarithmic scale in Figure 6. The extrapolated closed-system values of $\Sigma\Pi_{eq}$ for both the supersaturated and undersaturated solutions ($[Ca^{2+}]$ fixed at 10.28×10^{-3} mol kg^{-1} sw) are also represented. Finally, data from closed-system equilibration experiments of calcite carried out for periods in excess of 30 days (i.e., in excess of the time required for calcite to reach equilibrium under the experimental conditions, see Mucci, 1983) in the presence of various concentrations of Mn^{2+} (Table VI) are plotted as a function of log $X_{L(Mn)}$ in Figure 6.

Most peculiar are the data from the U-80/83 and U-86/89 series of experiments during which the Mn^{2+} concentrations decreased abruptly. This observation was initially thought to result from the precipitation of rhodo-

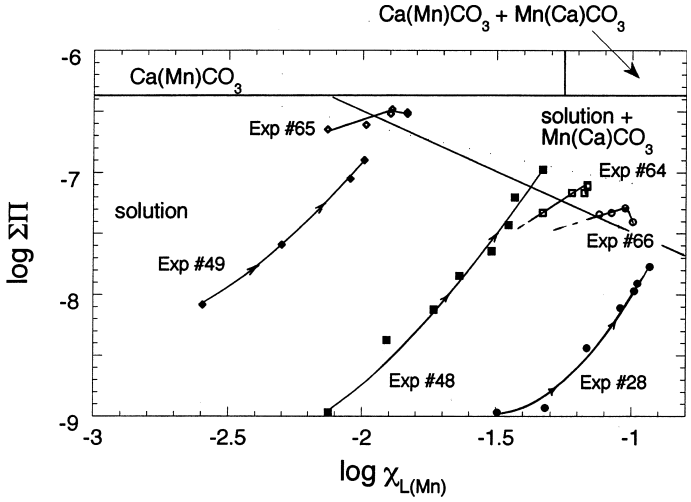

Figure 5. Representative solid solution-aqueous solution (SSAS) reaction paths for the open-system dissolution of natural kutnahorite (closed symbols) and synthetic pseudokutnahorite (open symbols) in seawater at 25 °C and various pCO_2s on a Lippmann diagram. Numbers refer to specific experiments (see Table IV).

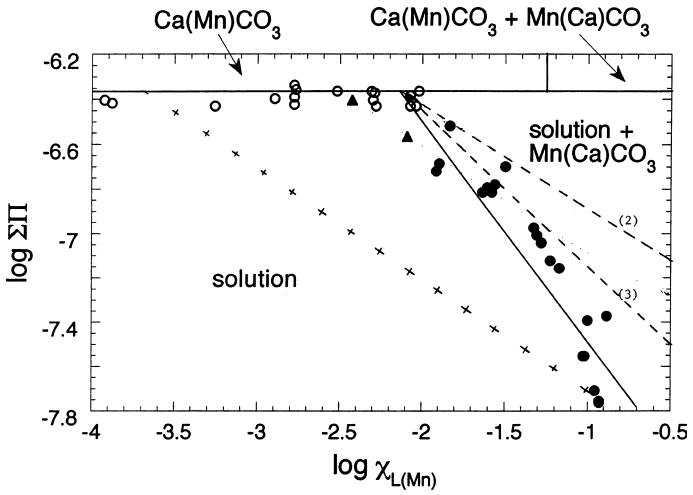

Figure 6. Steady-state total stoichiometric solubility products from the open-system (full dots) and closed-system (full diamonds) reactions of kutnahorite and pseudokutnahorite in seawater and the closed-system reactions of calcite (open dots) in the presence of various amounts of Mn(II) are overlain on an expanded and logarithmic Lippmann diagram. Dashed lines as in Figure 4b whereas the crossed dashed line is the pseudokutnahorite solutus (equation 24).

chrosite since the initial solutions (Table VI) were supersaturated with respect to rhodochrosite (i.e., $ICP_{rh} > K^*_{rh}$) and the solids recovered from these experiments were tinted with a pinkish brown overgrowth. However, upon further reaction, the solutions became highly undersaturated with respect to this mineral. A closer examination of the data (Table VI) reveals that as Mn^{2+} is taken up from the solution and Ca^{2+} is released to the solution. McBride (1979) observed a similar behavior in dilute solutions and proposed that it resulted from the following equilibrium reactions:

$$Mn^{2+} + HCO_3^- \longleftrightarrow MnCO_3 + H^+, \tag{22}$$

$$H^+ + CaCO_3 \longleftrightarrow Ca^{2+} + HCO_3^-, \tag{23}$$

Whereas McBride (1979) reported that Mn^{2+} uptake was approximately balanced by the release of Ca^{2+}, the data in Table VI (i.e., U-80 → U-81 → U-82 and U-87 → U-88) show that approximately two Ca^{2+} ions and one equivalent of alkalinity are released for each Mn^{2+} taken out of solution. Upon further reaction [Mn^{2+}], [Ca^{2+}], and A_t decrease as the solubility controlling phase, a manganoan calcite according to Figure 6, is precipitated. A similar behavior was observed by Böttcher (1997a) as aragonite was replaced by calcian rhodochrosites.

Table VI. Closed-system equilibration of calcite in seawater ($S = 35.0$) at 25 °C in the presence of dissolved Mn(II)

Exp.#	Time[a] (day)	$[Ca^{2+}]$ (mmol kg^{-1})	$[Mn^{2+}]$ (μmol kg^{-1})	A_t (meq kg^{-1})	A_c (meq kg^{-1})	pH (sws)	ICP_{cc} (10^{-7})	ICP_{rh} (10^{-9})	$\Sigma\Pi$ (10^{-7})
U-62	33	10.23	1.9	0.944	0.897	7.689	4.60[b]	0.756[c]	4.61[d]
U-63	117	10.15	16.8	1.016	0.975	7.630	4.39	0.747	4.40
U-64	308	10.32	17.1	0.966	0.926	7.612	4.08	0.676	4.09
U-65	924	10.15	16.9	0.958	0.920	7.586	3.78	0.630	3.79
U-68	33	10.24	53	0.902	0.854	7.705	4.32	2.12	4.34
U-63	117	10.10	50	0.927	0.882	7.667	4.27	2.18	4.29
U-64	308	10.30	52	0.966	0.928	7.595	3.94	1.94	3.96
U-65	924	10.27	53	0.929	0.891	7.586	3.70	1.92	3.72
U-74	33	10.27	97	0.922	0.877	7.669	4.34	4.10	4.38
U-75	117	10.19	31	0.998	0.956	7.633	4.35	1.31	4.36
U-76	308	10.31	85	0.938	0.901	7.576	3.68	3.05	3.71
U-77	924	10.31	94	0.899	0.860	7.603	3.71	3.38	3.74
U-80	33	10.27	260	0.749	0.708	7.631	3.23	8.23	3.31
U-81	117	10.47	88	1.148	1.115	7.521	4.11	3.46	4.15
U-82	308	10.64	13.5	1.172	1.141	7.490	4.00	0.510	4.01
U-83	924	10.49	1.25	0.964	0.926	7.589	3.95	0.047	3.95
U-86	33	10.10	498	0.842	0.803	7.605	3.42	16.9	3.59
U-87	117	10.02	479	0.862	0.824	7.587	3.34	16.0	3.50
U-88	308	10.99	6.05	1.249	1.223	7.407	3.70	0.204	3.70
U-89	924	10.74	1.42	0.978	0.942	7.557	3.85	0.052	3.85

[a]Time of equilibration.
[b]ICP_{cc}: Ion concentration product of $[Ca^{2+}][CO_3^{2-}]$ in $mol^2\ kg^{-2}$ sw.

Based on the results of the equilibration experiments and where they plot on the Lippmann diagram (Figure 6), it appears that for $X_{L(Mn)}$ greater than about 0.008 or $[Mn^{2+}] > 0.1$ mM (≈5 ppm) in seawater (i.e., for a fixed $[Ca^{2+}] = 10.28$ mM), the solubility controlling phase is a calcian rhodochrosite whereas for a smaller $X_{L(Mn)}$ a manganoan calcite is the solubility controlling-phase. Similarly, Böttcher (1997a), in an investigation of the transformation of aragonite to $Mn_xCa_{(1-x)}CO_3$ solid solutions in Ca–Mn chloride solutions, observed that a manganese-rich secondary carbonate (i.e., calcian rhodochrosite) formed from solutions whose initial $X_{L(Mn)} > 0.1$.

Based on the estimate of its stoichiometric solubility constant in seawater (see above), the pseudokutnahorite *solutus:*

$$\Sigma\Pi_{pkt} = \left\{ \frac{K^*_{pkt}}{\{X^*_{L(Mn)}(1 - X_{L(Mn)})\}} \right\}^{0.5} \tag{24}$$

would define a wedge that crosses the rhodochrosite *solutus* at low $X_{L(Mn)}$ (see Figure 6 in this paper and Figure 2 in Middelburg et al., 1987) and, thus, there may be a range of $X_{L(Mn)}$ over which this phase is stable. Results of this study, however, do not provide evidence for the existence of this stability field in seawater. In the presence of excess calcite surfaces and despite the formation of a manganese-rich phase (Figure 6), the solubility of Mn^{2+} in solution appears to be controlled by sorption (i.e., adsorption or co-precipitation) onto the calcite or the formation of a manganoan calcite.

Results of this study are adequately described by the regular solid solution model as all the experimental data conform with the *soluti* curves. Unfortunately, unless we assume ideal solid-solution behavior, there are only limited thermodynamic data (Böttcher, 1997b) to construct the complete set of *solidi* for the Lippmann diagrams and the composition of the solubility-controlling phases in these experiments cannot be readily determined because they are much too thin. Without the equilibrium solid compositions, the true equilibrium or stoichiometric saturation constants (Mucci and Morse, 1984; Plummer and Mackenzie, 1974; Thorstenson and Plummer, 1977), expressed as the product of the solution concentrations to a fractional exponent equal to the stoichiometry of the solid, cannot be calculated. The problem is further compounded by the fact that the composition of the solubility controlling phases may be dictated by its precipitation kinetics in the experimental systems. Several studies (Böttcher, 1998; Dromgoole and Walter, 1990; Lorens, 1981; Mucci, 1988; Pingitore et al., 1988) have shown that the partition coefficient of Mn^{2+} in calcite varies with the precipitation rate, decreasing with increasing rate.

4.2. CONTROL OF MANGANESE CONCENTRATION IN MARINE POREWATERS

4.2.1. Early Diagenetic Behavior Through the Redox Zones

The concentration of manganese in sediment porewaters is controlled by either equilibrium with a solid phase or reaction kinetics. In the first case, the equilibrium may be dictated by the solubility of a solid phase, a distinct manganese mineral or solid solution, or by adsorption to a pre-existing or authigenic phase. In the second case, the relative rates of reactions that release Mn(II) to porewaters, its diffusion, and the formation of authigenic phases will be critical. These reactions may be microbially mediated as well as catalysed or inhibited by the presence of metabolites. For example, the presence of phosphate will inhibit the precipitation of carbonate minerals (e.g., Burton and Walter, 1990; Mucci 1986) including rhodochrosite from seawater, and may lead to large porewater supersaturations with respect to these minerals (Berner et al., 1978; Mucci and Edenborn, 1992). The following discussion will be restricted to equilibrium processes.

In oxic marine sediments, the formation of authigenic Mn(III,IV) oxides and oxyhydroxides controls the solubility of manganese in marine porewaters. These oxides and oxyhydroxides are insoluble within the pH range (i.e., 7–8.5) normally encountered in marine sediments. They are easily reduced and release Mn(II) to the porewaters following burial below the oxygen penetration depth (e.g., Burdige, 1993). Consequently, strong concentration gradients are established which induce diffusion of Mn(II) back to the oxic zone where it can be oxidized and precipitated as an oxide in the form of a colloidal suspension, mineral coating, or nodule. The oxidation of Mn(II) is relatively slow and autocatalytic (Wilson, 1980). Furthermore, as a consequence of oscillations of the oxygen penetration depth due to episodic inputs of reactive organic matter to the sediments (Gobeil et al., 1998), the oxides are often found above the oxygen penetration depth and dissolved Mn(II) is frequently encountered in the oxic zone and may even escape to overlying waters (Balzer, 1982; Sundby et al., 1986).

Under suboxic or anoxic conditions, Mn(II) concentrations generally increase with depth before they level out or decrease (e.g., Burdige, 1993; Sawlan and Murray, 1983; Shaw et al., 1990). Highly variable levels of downcore porewater Mn(II) have been reported in marine sedimentary environments (0.5–400 μmol kg^{-1}; Middelburg et al., 1987 and references therein). The generation of carbonate alkalinity resulting from sulfate reduction and methanogenesis will generally promote the precipitation of a carbonate phase. Various authigenic carbonate Mn-bearing solid phases have been proposed as solubility controlling phases (see discussion below) but the porewater Mn(II) concentrations often exceed the solubility of these minerals, particularly in coastal, terrigeneous sediments (e.g., Berner et al., 1970;

Gratton et al., 1990; Kremling, 1983; Mucci and Edenborn, 1992). In coastal, siliciclastic marine sediments, the absence of a suitable substrate (i.e., solid carbonate) and the presence of relatively high concentrations of inhibitors (e.g., dissolved organic carbon and phosphate) may impede carbonate mineral nucleation and growth until very high saturations are reached. For example, in highly reducing marine terrigenous sediments where sulfate becomes depleted and some reactive iron phases persist, vivianite ($Fe_3(PO_4)_2 \cdot 8H_2O$) rather than siderite ($FeCO_3$) or ankerite ($CaFe(CO_3)_2$) precipitates in spite of the high saturation state of the porewaters with respect to the metal carbonate minerals (Martens et al., 1978; Mucci et al., 2000). Reactive manganese phases often do not survive the transition (and cycling) through the oxic–suboxic–sulfidic zones and, thus, the precipitation of a manganese carbonate in the fermentation zone of a marine sediment is unlikely.

Mn(II) sulfides rarely form under sulfidic conditions because the sulfide activity is most commonly buffered by the precipitation of iron sulfides. MnS has been observed in the sediments of the Baltic Sea (Suess, 1979) where, as indicated below, exceptionally high porewater Mn(II) concentrations are found. Small amounts of Mn(II) can adsorb to iron monosulfides (mackinawite; Arakaki and Morse, 1996). The adsorbed and co-precipitated Mn(II) is apparently released back to solution upon the conversion of monosulfides to pyrite (Luther et al., 1980) but is not likely to contribute significantly to the porewater Mn(II) pool.

4.2.2. Authigenic Carbonate Phases

As revealed by the present study, the nature and composition of the manganese carbonate phases that may precipitate from seawater under suboxic/anoxic conditions are dictated by the porewater $[Mn^{2+}]$:$[Ca^{2+}]$ ratio, the abundance of calcite surfaces and reaction kinetics (e.g., manganic mineral dissolution and manganous mineral precipitation inhibition). The adsorption of Mn(II) on calcite surfaces can buffer the porewater Mn(II) concentration. Michard (1971) and Thomson et al. (1986) noted that sorption of Mn(II) on calcium carbonate surfaces was important in determining the diffusive flux of Mn(II) from anoxic sediments and it was suggested that this process may be responsible for the scarcity of manganese nodules in calcareous sediments (Boyle, 1983; Martin and Knauer, 1983; Piper and Williamson, 1977). In fact, results of the closed-system equilibration experiments with calcite (see U-80–U-89 in Table VI) indicate that, if enough calcite surfaces are available, adsorption or co-precipitation (i.e., formation of a manganoan calcite) onto the calcite surface can lower the aqueous Mn(II) concentration below that expected for saturation with respect to rhodochrosite (Franklin and Morse, 1983; McBride, 1979; Wartel et al., 1990).

Estimates of the partition coefficients of Mn(II) in calcite were derived from field and laboratory measurements. Observed and selected values range between 1.5 and 51 (Bodine et al., 1965; Böttcher, 1998; Ichikuni, 1973; Kumagai, 1978; Michard, 1968; Mucci, 1988; Pingitore, 1978; ten Have and Heijnen, 1985) but few of these studies indicate the compositional range over which the solid solution can form. Furthermore, several studies (Böttcher, 1998; Dromgoole and Walter, 1990; Lorens, 1981; Mucci, 1988; Pingitore et al., 1988) confirmed that the partition coefficient decreases with increasing precipitation rate. The validity and application of these partition coefficients has recently been questioned given that at least two processes have been identified which lead to non-uniform partitioning of trace elements during abiotic calcite growth (Rimstidt et al., 1998): a surface-site specific process resulting in sectoral and intrasectoral zoning (Reeder and Grams, 1987; Reeder and Paquette, 1989; Paquette and Reeder, 1995) and a boundary-layer process resulting in oscillatory zoning (Reeder et al., 1990; Wang and Merino, 1992).

In calcite-poor sediments, calcian rhodochrosites may precipitate and determine the Mn(II) solubility. These minerals would only form at modest to high $[Mn^{2+}]$:$[Ca^{2+}]$ ratios (or $X_{L(Mn)} > 0.01$). The ratios required for calcian rhodochrosite precipitation could be reached when authigenic oxide coatings undergo reductive dissolution following burial below the oxygen penetration zone (Calvert and Pedersen, 1996) or under exceptional conditions such as those encountered in the marine muds of the Baltic Sea where high concentrations of Mn(II) ([Mn(II)] = 100–500 μM; Jakobsen and Postma, 1989; Kulik et al., 2000; Lepland and Stevens, 1998) are believed to result from the dissolution of nodular manganese oxyhydroxides upon the onset of anoxic conditions between episodic flushings by well-oxygenated North Sea water (Huckriede and Meischner, 1996; Sternbeck and Sohlenius, 1997). The $X_{L(Mn)}$ in the marine porewaters of the top 1 m of the marine muds of the Gotland and Landsort Deeps varies between 0.06 and 0.12 (Jakobsen and Postma, 1989), well within the stability field of calcian rhodochrosites (Figure 5). On the other hand, the composition of authigenic calcian rhodochrosites recovered from Baltic Sea sediments fall between $0.48 < X_{S(Mn)} < 0.84$, with an average around 0.7 (Kulik et al., 2000; Lepland and Stevens, 1998), well within the miscibility gap. Calcian rhodochrosites in these settings have also been observed to form on detrital dolomite cores and recrystallized shell fragments (Jakobsen and Postma, 1989; Manheim, 1982; Suess, 1979). Although the formation of kutnahorite or pseudokutnahorite from marine porewaters has been proposed (Calvert and Pedersen, 1996; Calvert and Price, 1970; Lynn and Bonatti, 1965; Pedersen and Price, 1982), results of this study indicate that, whereas a phase approximating the composition of these minerals may precipitate from seawater, it would not display the same stability in solution.

5. Conclusions

The solubility product of a calcian rhodochrosite approximating the stoichiometry of natural kutnahorite, a pseudokutnahorite, was measured in deionized distilled water at 25 °C, one atmosphere total pressure, and various pCO_2s. With a $pK^{o}_{pkt} = 20.77$ (± 0.03), its thermodynamic solubility product is almost 11 times larger than that of its ordered counterpart, kutnahorite ($pK^{o}_{kt} = 21.81 \pm 0.07$). Since the ordered mineral cannot readily precipitate from a low temperature aqueous solution (i.e., the reaction is kinetically inhibited), the solubility of the disordered mineral will ultimately determine the IAP of the solution in the presence of the former.

The stoichiometric solubility constants of calcite and rhodochrosite in seawater were used to construct Lippmann phase diagrams and define their respective fields of stability in the presence of Mn^{2+}. Experimental data from this study and field observations are consistent with the interpretations based on these diagrams and indicate that, for a given $[Mn^{2+}]$:$[Ca^{2+}]$ ratio (or $X_{L(Mn)}$), one of the two authigenic phases(i.e., a manganoan calcite or calcian rhodochrosite) will likely control the solubility of manganese in suboxic marine environments when these can be nucleated and grow. In a calcite-rich sediment, however, the co-precipitation and adsorption of Mn(II) on the surface of calcite will determine the dissolved manganese concentration.

Acknowledgements

The author would like to express his gratitude to Mr. John L. Baum and Richard Hauck for providing samples of natural kutnahorite from Sterling Mines, New Jersey. The technical assistance of Constance Guignard and stimulating discussions with Dr. Jacqueline Windh were greatly appreciated. Finally, the author is indebted to Profs. H. Gamsjäger, F. Mackenzie, J.W. Morse and an anonymous reviewer who provided critical comments and advice on this and previous versions of this paper. Financial support for this research was provided by the Natural Sciences and Engineering Research Council of Canada (NSERC) to the author. Additional funds from NSERC and FCAR to the GEOTOP-McGill-UQAM research center through infrastucture and center grants allowed the completion this study.

References

Arakaki T. and Morse J. W. (1996) Coprecipitation and adsorption of Mn(II) with mackinawite (FeS) under conditions similar to those found in anoxic sediments. *Geochim. Cosmochim. Acta* **57,** 9–14.

Ball J. W., Nordstrom D. K. and Jenne E. A. (1980) Additional and revised thermochemical data and computer code for WATEQ2-A computerized chemical model for trace and major

element speciation and mineral equilibria of natural waters. *U.S. Geol. Surv., Water-Resour. Invest. Rept*. 78–116, 109p.

Balzer W. (1982) On the distribution of iron and manganese at the sediment/water interface: Thermodynamic vs. kinetic control. *Geochim. Cosmochim. Acta* **46**, 1153–1161.

Bates R. G. (1973) *Determination of pH*, 2nd edn., John Wiley & Sons, New York.

Berner R. A., Scott M. R. and Thomlinson C. (1970) Carbonate alkalinity in pore waters of anoxic marine sediments. *Limnol. Oceanogr*. **15**, 544–549.

Berner R. A., Westrich J. T., Graber R., Smith J. and Martens C. S. (1978) Inhibition of aragonite precipitation from supersaturated seawater. *Amer. J. Sci*. **278**, 816–837.

Bodine M. W., Holland H. D. and Borczik M. (1965) Coprecipitation of manganese and strontium with calcite. In: *Problems of Postmagmatic Ore Deposition, Proc. Symp., Prague,* Vol. 2, pp. 401–406.

Böttcher M. E. (1997a) The transformation of aragonite to $Mn_xCa_{(1-x)}CO_3$ solid-solutions at 20 °C: An experimental study. *Mar. Chem*. **57**, 97–106.

Böttcher M. E. (1997b) Experimental dissolution of $CaCO_3$-$MnCO_3$ solid solutions in CO_2-H_2O solutions at 20 °C. *Solid State Ionics* **101–103**, 1263–1266.

Böttcher M. E. (1998) Manganese(II) partitioning during experimental precipitation of rhodochrosite-calcite solid-solutions from aqueous solutions. *Mar. Chem*. **62**, 287–297.

Boyle E. A. (1983) Manganese carbonate overgrowths on foraminifera tests. *Geochim. Cosmochim. Acta* **47**, 1815–1819.

Boynton W. V. (1971) *An Investigation of the Thermodynamics of Calcite–Rhodochrosite Solid Solutions*. M.Sc. thesis, Carnegie-Melon University, 147 pp.

Burdige D. J. (1993) The biogeochemistry of manganese and iron reduction in marine sediments. *Earth–Science Reviews* **35**, 249–284.

Burton E. and Walter L. M. (1990) The role of pH in phosphate inhibition of calcite and aragonite precipitation rates in seawater. *Geochim. Cosmochim. Acta* **54**, 797–808.

Calvert S. E. and Pedersen T. F. (1996) Sedimentary geochemistry of manganese: Implications for the environment of formation of manganiferous black shales. *Econ. Geol*. **91**, 36–47.

Calvert S. E. and Price N. B. (1970) Composition of manganese nodules and manganese carbonates from Loch Fyne, Scotland. *Contrib. Mineral. Petrol*. **29**, 215–233.

Capobianco C. and Navrotsky A. (1987) Solid-solution thermodynamics in $CaCO_3$–$MnCO_3$. *Amer. Mineral*. **72**, 312–318.

Clarke E. T., Loeppert R. H. and Ehrman J. M. (1985) Crystallization of iron oxides on calcite surfaces in static systems. *Clays and Clay Minerals* **33**, 152–158.

de Capitani C. and Peters T. (1981) The solvus in the system $MnCO_3$–$CaCO_3$. *Contrib. Mineral. Petrol*. **76**, 394–400.

De Lange G. J. (1986) Early diagenetic reactions in interbedded pelagic and turbidic sediments in the Nares Abyssal Plain (western North Atlantic): Consequences for the composition of sediment and interstitial water. *Geochim. Cosmochim. Acta* **50**, 2543–2561.

Dickson A. G. (1981) An exact definition for total alkalinity and a procedure for the estimation of alkalinity and total inorganic carbon from titration data. *Deep-Sea Res*. **6**, 609–623.

Dickson A. and Millero F. J. (1987) A comparison of the equilibrium constants for the dissociation of carbonic acid in seawater media. *Deep-Sea Res*. **34**, 1733–1743.

Dromgoole E. L. and Walter L. M. (1990) Iron and manganese incorporation into calcite: Effects of growth kinetics, temperature and solution chemistry. *Chem. Geol*. **81**, 311–336.

Emerson S. E., Jahnke R., Bender M., Froelich P., Klinkhammer G., Bowser C. and Setlock G. (1980) Early diagenesis in sediments from the eastern equatorial Pacific. I. Pore water nutrient and carbonate results. *Earth Planet. Sci. Lett*. **49**, 57–80.

Franklin M. L. and Morse J. W. (1983) The interaction of manganese(II) with the surface of calcite in dilute solutions and seawater. *Mar. Chem.* **12**, 241–254.

Frondel C. and Bauer L. H. (1955) Kutnahorite: A manganese dolomite, $CaMn(CO_3)_2$. *Amer. Mineral.* **40**, 748–760.

Fubini B. and Stone F. S. (1983) Physico-chemical properties of $MnCO_3$–$CaCO_3$ and MnO–CaO solid solutions. *J. Chem. Soc. Faraday Trans. Ser. l.* **79**, 1215–1227.

Gammons C. and Seward T. M. (1996) Stability of manganese (II) chloride complexes from 25 to 300 °C. *Geochim. Cosmochim. Acta* **60**, 4295–4311.

Gamsjäger H., Königsberger E. and Preis W. (2000) Lippmann diagrams: Theory and application to carbonate systems. *Aquat. Geochem.* **6**, 119–132.

Garrels R. M. and Thompson M. E. (1962) A chemical model for seawater at 25 °C and one atmosphere total pressure. *Amer. J. Sci.* **260**, 57–66.

Garrels R. M., Thompson M. E. and Siever R. (1960) Stability of some carbonates at 25 °C and one atmosphere total pressure. *Amer. J. Sci.* **258**, 402–418.

Garrels R. M., Thomson M. E. and Siever R. (1961) Control of carbonate solubility by carbonate complexes. *Amer. J. Sci.* **259**, 24–45.

Glynn P. D. and Reardon E. (1990) Solid-solution aqueous-solution equilibria: Thermodynamic theory and representation. *Amer. J. Sci.* **290**, 164–201.

Glynn P. D., Reardon E. J., Plummer L. N. and Busenberg E. (1990) Reaction paths and equilibrium end-points in solid-solution aqueous-solution systems. *Geochim. Cosmochim. Acta* **54**, 267–282.

Gobeil C., Macdonald R. W. and Sundby B. (1998) Diagenetic separation of cadmium and manganese in suboic continental margin sediments. *Geochim. Cosmochim. Acta* **61**, 4647–4654.

Goldsmith J. R. (1983) Phase relations of rhombohedral carbonates. In: *Carbonates: Mineralogy and Chemistry* (ed. J.R. Reeder). *Rev. Mineral.* **11**, pp. 49–96.

Goldsmith J. R. and Graf D. L. (1957) The system CaO–MnO–CO_2: Solid solution and decomposition relations. *Geochim. Cosmochim. Acta* **11**, 310–334.

Goldsmith J. R. and Graf D. L. (1960) Subsolidus relations in the system $CaCO_3$–$MgCO_3$–$MnCO_3$. *J. Geol.* **68**, 324–335.

Goyet C. and Poisson A. (1989) New determination of carbonic acid dissociation constants in seawater as a function of temperature and salinity. *Deep-Sea Res.* **36**, 1635–1654.

Gratton Y., Edenborn H. M., Silverberg N. and Sundby B. (1990) A mathematical model for manganese diagenesis in bioturbated sediments. *Amer. J. Sci.* **290**, 246–262.

Hansson I. (1973) A new set of acidity constants for carbonic acid and boric acid in seawater. *Deep–Sea Res.* **20**, 461–478.

Huckriede H. and Meischner D. (1996) Origin and environment of manganese-rich sediments within black-shale basins. *Geochim. Cosmochim. Acta* **60**, 1399–1413.

Ichikuni M. (1973) Partition of strontium between calcite and solution: Effect of substitution by manganese. *Chem. Geol.* **11**, 315–319.

Iwafuchi K., Watanabe C. and Otsuka R. (1983) Thermal decomposition of magnesian kutnahorite. *Thermochim. Acta* **60**, 361–381.

Jakobsen R. and Postma D. (1989) Formation and solid solution behavior of Ca–rhodochrosites in marine muds of the Baltic deeps. *Geochim. Cosmochim. Acta* **53**, 2639–2648.

Johnson K. S. (1982) Solubility of rhodochrosite ($MnCO_3$) in water and seawater. *Geochim. Cosmochim. Acta* **46**, 1805–1809.

Kester D. R., Duedall I. W., Connors D. N. and Pytkowicz R. M. (1967) Preparation of artificial seawater. *Limnol. Oceanogr.* **12**, 176–178.

Kornicker W. A., Presta P. A., Paige C. R., Johnson D. M., Hileman Jr. O. E. and Snodgrass W. J. (1991) The aqueous dissolution kinetics of the barium/lead sulfate solid solution series at 25 and 60 °C. *Geochim. Cosmochim. Acta* **55**, 3531–3541.

Kremling K. (1983) The behavior of Zn, Cd, Cu, Ni, Co, Fe, and Mn in anoxic Baltic sediments. *Mar. Chem.* **13**, 87–108.

Kulik D. A., Kernten M., Heiser U. and Neumann T. (2000) Application of Gibbs energy minimization to model early-diagenetic solid-solution aqueous-solution equilibria involving authigenic rhodochrosites in anoxic Baltic Sea sediments. *Aquat. Geochem.* **6**, 147–199.

Kumagai T. (1978) Coprecipitation of manganese with calcium carbonate. *Bull. Inst. Chem. Res. Kyoto Univ.* **56**, 280–285.

Lebel J. and Poisson A. (1976) Potentiometric determination of calcium and magnesium in seawater. *Mar. Chem.* **4**, 321–332.

Lepland A. and Stevens R. L. (1998) Manganese authigenesis in the Landsort Deep, Baltic Sea. *Mar. Geol.* **151**, 1–25.

Lesht D. and Bauman J. E. Jr. (1978) Thermodynamics of the manganese (II) bicarbonate system. *Inorg. Chem.* **17**, 3332–3334.

Lippmann F. (1980) Phase diagrams depicting aqueous solubility on binary mineral systems. *Neues Jahrb. Mineral. Abh.* **139**, 1–25.

Lippmann F. (1982) Stable and metastable solubility diagrams for the system $CaCO_3$–$MgCO_3$–H_2O at ordinary temperature. *Bull. Minéral.* **105**, 273–279.

Loeppert R. H. and Hossner L. R. (1984) Reactions of Fe^{2+} and Fe^{3+} with calcite. *Clays and Clay Minerals* **32**, 213–222.

Lorens R. B. (1981) Sr, Cd, Mn and Co distribution coefficients in calcite as a function of calcite precipitation rate. *Geochim. Cosmochim. Acta* **45**, 553–561.

Luther G. W. III., Meyerson A. L., Krajewski J. J. and Hires R. (1980) Metal sulfides in estuarine sediments. *J. Sediment. Petrol.* **50**, 1117–1120.

Lynn D. C. and Bonatti E. (1965) Mobility of manganese in diagenesis of deep-sea sediments. *Mar. Geol.* **3**, 457–474.

Manheim F. T. (1982) Geochemistry of manganese carbonates in the Baltic Sea. *Stockholm Contrib. Geol.* **37**, 145–159.

Martens C. S., Berner R. A. and Rosenfeld J. K. (1978) Interstitial water chemistry of anoxic Long Island Sound sediments. 2. Nutrient regeneration and phosphate removal. *Limnol. Oceanogr.* **23**, 605–617.

Martin J. H. and Knauer G. E. (1983) VERTEX: Manganese transport with $CaCO_3$. *Deep-Sea Res.* **30**, 411–425.

McBeath J. K., Rock P. A., Casey W. H. and Mandell G. K. (1998) Gibbs energies of formation of metal-carbonate solid solutions: Part 3. The $Ca_xMn_{1-x}CO_3$ system at 298 K and 1 bar. *Geochim. Cosmochim. Acta* **62**, 2799–2808.

McBride M. B. (1979) Chemisorption and precipitation of Mn^{2+} at $CaCO_3$ surfaces. *Soil Sci. Soc. Amer. J.* **43**, 693–698.

Merhbach C., Culberson C. H., Hawley J. E. and Pytkowicz R. M. (1973) Measurements of the apparent dissociation constants of carbonic acid in seawater at atmospheric pressure. *Limnol. Oceanogr.* **18**, 897–907.

Mettler S. (2002) *In Situ Iron Removal from Ground Water: Fe(II) Oxygenation, and Precipitation Products in a Calcareous Aquifer*. Doctoral thesis, Swiss Federal Institute of Technology, Zürich.

Michard G. (1968) Coprécipitation de l'ion manganeux avec le carbonate de calcium. *C. R. Acad. Sci., Sér. D.* **267**, 1685–1688.

Michard G. (1971) Theoretical model for manganese distribution in calcareous sediment cores. *J. Geophys. Res.* **76**, 2179–2186.

Middelburg J. J., de Lange G. J. and van der Weijden C. (1987) Manganese solubility control in marine pore waters. *Geochim. Cosmochim. Acta* **51**, 759–763.

Millero F. J. (1974) The physical chemistry of seawater. *Ann. Rev. Earth Planet. Sci. Lett.* **2**, 101–150.

Millero F. J. (1979) The thermodynamics of the carbonate system in seawater. *Geochim. Cosmochim. Acta* **43**, 1651–1661.

Millero F. J., Zhang J. -Z., Fiol S., Sotolongo S., Roy R. N., Lee K. and Mane S. (1993) The use of buffers to measure the pH of seawater. *Mar. Chem.* **44**, 143–152.

Mucci A. (1983) The solubility of calcite and aragonite in seawater at various salinities, temperatures, and one atmosphere total pressure. *Amer. J. Sci.* **283**, 780–799.

Mucci A. (1986) Growth kinetics and composition of magnesian calcite overgrowths precipitated from seawater: Quantitative influence of orthophosphate ions. *Geochim. Cosmochim. Acta* **50**, 2255–2265.

Mucci A. (1988) Manganese uptake during calcite precipitation from seawater: Conditions leading to the formation of a pseudokutnahorite. *Geochim. Cosmochim. Acta* **52**, 1859–1868.

Mucci A. (1991) The solubility and free energy of formation of natural kutnahorite. *Can. Mineral.* **29**, 113–121.

Mucci A. and Edenborn H. M. (1992) Influence of an organic-poor landslide deposit on the early diagenesis of iron and manganese in a coastal marine sediment. *Geochim. Cosmochim. Acta* **56**, 3909–3921.

Mucci A. and Morse J. W. (1984) The solubility of calcite in seawater solutions of various magnesium concentration, $I_t = 0.697$ m at 25 °C and one atmosphere total pressure. *Geochim. Cosmochim. Acta* **48**, 815–822.

Mucci A., Richard L. -F., Lucotte M. and Guignard C. (2000) The differential geochemical behavior of arsenic and phosphorus in the water column and sediments of the Saguenay Fjord Estuary, Canada. *Aquat. Geochem.* **6,** 293–324.

Paquette J. and Reeder R. (1995) Relationship between surface structure, growth mechanism, and trace element incorporation in calcite. *Geochim. Cosmochim. Acta* **59**, 735–749.

Peacor D. R., Essene E. J. and Gaines A. M. (1987) Petrologic and crystal-chemical implications of cation order-disorder in kutnahorite [$CaMn(CO_3)_2$]. *Amer. Mineral.* **72**, 319–328.

Pedersen T. F. and Price N. B. (1982) The geochemistry of manganese carbonate in Panama Basin sediments. *Geochim. Cosmochim. Acta* **46**, 59–68.

Pingitore N. E. (1978) The behavior of Zn^{2+} and Mn^{2+} during carbonate diagenesis: Theory and applications. *J. Sediment. Petrol.* **48**, 799–814.

Pingitore N. E., Eastman M. P., Sandige M., Oden K. and Freiha B. (1988) The coprecipitation of manganese (II) with calcite: An experimental study. *Mar. Chem.* **25**, 107–120.

Piper D. Z. and Williamson M. E. (1977) Composition of Pacific Ocean ferromanganese nodules. *Mar. Geol.* **23**, 285–303.

Plummer L. N. and Busenberg E. (1982) The solubilities of calcite, aragonite and vaterite in CO_2–H_2O solutions between 0 and 90 °C, and an evaluation of the aqueous model for the system $CaCO_3$–CO_2–H_2O. *Geochim. Cosmochim. Acta* **46**, 1011–1040.

Plummer L. N. and Mackenzie F. T. (1974) Predicting mineral solubility from rate data. Application to the dissolution of magnesium calcites. *Amer. J. Sci.* **274**, 61–83.

Plummer L. N., Jones B. F. and Truesdell A. H. (1976) WATEQF-A FORTRAN IV version of WATEQ, a computer program for calculating chemical equilibrium of natural waters. *U.S. Geol. Surv. Water Resources Inv. Rept.* 76–13, 71p.

Reeder R. J. and Grams J. C. (1987) Sector zoning in calcite cement crystals: Implications for trace element distributions in carbonates. *Geochim. Cosmochim. Acta* **51**, 187–194.

Reeder R. J. and Paquette J. (1989) Sector zoning in natural and synthetic calcites. *Sediment. Geol.* **65**, 239–247.

Reeder R. J., Fagioli R. O. and Meyers W. J. (1990) Oscillatory zoning of manganese in solution-grown calcite crystals. *Earth-Science Rev.* **29**, 39–46.

Rimstidt J. D., Balog A. and Webb J. (1998) Distribution of trace elements between carbonate minerals and aqueous solutions. *Geochim. Cosmochim. Acta* **62**, 1851–1863.

Robie R. A., Hemingway B. S., and Fisher J. R. (1978) *Thermodynamic properties of minerals and related substances at 298.15 K and 1 bar (10^5 pascals) pressure and at higher temperatures. U.S. Geol. Surv. Bull.* **1452**, 456pp.

Roy R. N., Roy L. N., Vogel K. M., Porter-Moore C., Pearson T, Good C. E., Millero F. J. and Campbell D. M. (1993) The dissociation constants of carbonic acid in seawater at salinities 5 to 45 and temperatures 0 to 45 °C. *Mar. Chem.* **44**, 249–267.

Sawlan J. J, and Murray J. W. (1983) Trace metal remobilization in the interstitial waters of red clay and hemipelagic marine sediments. *Earth Planet. Sci. Lett.* **64**, 213–230.

Sayles F. L. (1981) The composition and diagenesis of interstitial solutions. II. Fluxes and diagenesis at the water-sediment interface in the high latitude North and South Atlantic. *Geochim. Cosmochim. Acta* **45**, 1061–1086.

Sayles F. L. (1985) $CaCO_3$ solubility in marine sediments: Evidence for equilibrium and non-equilibrium behavior. *Geochim. Cosmochim. Acta* **49**, 877–888.

Shaw T. J., Gieskes J. M. and Jahnke R. A. (1990) Early diagenesis in differing depositional environments: The response of transition metals in pore water. *Geochim. Cosmochim. Acta* **54**, 1233–1246.

Sternbeck J. and Sohlenius G. (1997) Authigenic sulfide and carbonate mineral formation in Holocene sediments of the Baltic Sea. *Chem. Geol.* **135**, 55–73.

Suess E. (1979) Mineral phases formed in anoxic sediments by microbial decomposition of organic matter. *Geochim. Cosmochim. Acta* **43**, 339–352.

Sundby B., Anderson L. G., Hall P. O. J., Iverfeldt A., Rutgers van der Loeff M. M. and Westerlund S. F. G. (1986) The effect of oxygen on release and uptake of cobalt, manganese, iron and phosphate at the sediment-water interface. *Geochim. Cosmochim. Acta* **50**, 1281–1288.

ten Have T. and Heijnen W. (1985) Cathodoluminescence activation and zonation in carbonate rocks: An experimental approach. *Geol. Mijnbouw* **64**, 297–310.

Thomson J., Higgs N. C., Jarvis I., Hydes D. J., Colley S. and Wilson T. R. R. (1986) The behaviour of manganese in Atlantic carbonate sediments. *Geochim. Cosmochim. Acta* **50**, 1807–1818.

Thorstenson D. C. and Plummer N. L. (1977) Equilibrium criteria for two-component solids reacting with fixed composition in an aqueous phase–example the magnesian calcites. *Amer. J. Sci.* **277**, 1203–1223.

Wang Y. and Merino E. (1992) Dynamic model of oscillatory zoning of trace elements in calcite: Double layer, inhibition, and self-organisation. *Geochim. Cosmochim. Acta* **56**, 587–596.

Wartel M., Skiker M., Auger Y. and Boughriet A. (1990) Interaction of manganese(II) with carbonates in seawater: Assessment of the solubility product of $MnCO_3$ and Mn distribution coefficients between the liquid phase and $CaCO_3$ particles. *Mar. Chem.* **29**, 99–117.

Wildeman T. R. (1969/1970) The distribution of Mn^{2+} in some carbonates by electron paramagnetic resonance. *Chem. Geol.* **5**, 167–177.

Wilson D. E. (1980) Surface and complexation effects on the rate of Mn(II) oxidation in natural waters. *Geochim. Cosmochim. Acta* **44**, 1311–1317.